Solid State Phenomena Vols. 205-206 (2014) pp 26-33

doi:10.4028/www.scientific.net/SSP.205-206.26

External and internal gettering of interstitial iron in silicon for solar cells

Daniel Macdonald[1, a], An Yao Liu[1,b] and Sieu Pheng Phang[1,c]

[1]Research School of Engineering, College of Engineering and Computer Science, The Australian National University, Canberra, ACT 0200, Australia.

[a]daniel.macdonald@anu.edu.au (corresponding author), [b]anyao.liu@anu.edu.au, [c]pheng.phang@anu.edu.au

Keywords: silicon, iron, gettering, precipitation, solar cells

Abstract. The removal of dissolved iron from the wafer bulk is important for the performance of p-type multicrystalline silicon solar cells. In this paper we review some recent progress in understanding both external and internal gettering of iron. Internal gettering at grain boundaries and dislocations occurs naturally during ingot cooling, and can also be driven further during cell processing, especially by moderate temperature anneals (usually below 700 °C). Internal gettering at intra-grain defects plays key a role during such precipitation annealing. External gettering to phosphorus diffused regions is crucial in reducing the dissolved iron concentration during cell processing, although its effectiveness depends strongly on the diffusion temperature and profile. Gettering of Fe by boron and aluminum diffusions is also found to be very effective under certain conditions.

Introduction

Gettering of iron in multicrystalline silicon wafers is crucial for achieving reasonable cell efficiencies, since the recombination activity of dissolved interstitial iron is very high in standard p-type wafers. Such gettering can occur internally, leading to precipitation of dissolved Fe at structural defects such as dislocations and grain boundaries, usually resulting in a reduction of the overall impact of the iron on the effective lifetime of the sample. External gettering of Fe to diffused regions at the wafer surfaces, which occurs during cell fabrication, is also critical for reducing the interstitial Fe concentration. This is most often achieved via phosphorus diffusions, although boron and aluminium diffusions can also provide very effective Fe gettering, under the right conditions. In this paper, we provide an overview of our recent work on both external and internal gettering of Fe in crystalline silicon wafers. Firstly however, we review some relevant properties of Fe in silicon, and some common methods used to detect dissolved interstitial Fe in silicon wafers.

Properties of iron in silicon

Iron is one of the most common transition metal impurities in wafer-based silicon solar cells. It is especially important in multicrystalline silicon wafers, in which it occurs primarily due to contamination from the crucible during ingot growth [1,2]. Typical concentrations of Fe in directionally-solidified multicrystalline ingots are 10^{13} - 10^{14} cm^{-3} in the central regions, and up to 10^{15} cm^{-3} near the bottom and top of the ingots [3,4], due to impurity segregation and solid-state in-diffusion of Fe from the crucible walls.

Comparisons of the total Fe concentrations and dissolved Fe concentrations [4] have shown that the vast majority of the Fe (>95%) is usually present in precipitated form. These precipitates predominantly occur as iron silicide particles located at grain boundaries and dislocation clusters, and less frequently as iron silicate inclusions which may be present within the grains [1,5]. The remaining few per cent is present as dissolved Fe in the interstitial form. These interstitial Fe atoms are mobile even at room temperature, and courtesy of their positive charge state in p-type silicon,

Table 1. *Selected energy levels E_T and capture cross sections for electrons σ_n and holes σ_p of Fe-related centres.*

Centre	E_T [eV]	σ_n [cm^2]	σ_p [cm^2]	Ref.
Fe_i	E_V+0.48	1.3×10^{-14}	7×10^{-17}	[7,9]
FeB	E_C-0.26	5×10^{-15}	3×10^{-15}	[7,8]
FeGa	E_V+0.2	4×10^{-14}	2×10^{-14}	[6]
FeIn	E_V+0.15	3.5×10^{-13}	1.5×10^{-14}	[6]

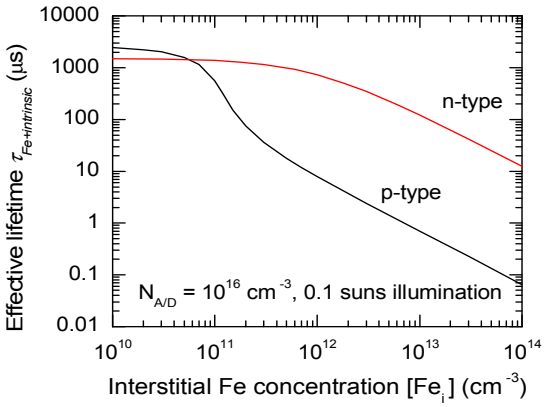

Fig 1. *Effective lifetimes in n- and p-type Si as a function of the interstitial Fe concentration [Fe_i].*

bond with negatively charged ionized dopant atoms in p-type silicon, usually boron, thus forming FeB pairs, although FeGa, FeIn and FeAl pairs can also occur [6].

The chemical state of Fe in silicon plays a key role in determining its recombination activity, which is of primary importance for solar cell performance. The recombination activity of precipitated Fe is difficult to specify, due to the fact that precipitates can vary greatly in size, may be present in a surrounding lattice with different degrees of imperfection, stress or strain, and also present a distribution of energy states in the band-gap, rather than a single energy level. However, the energy levels and capture cross sections of the recombination centres associated with interstitial Fe and its acceptor pairs have been fairly well documented. A selection of these are summarized in Table 1 from Refs [6-9]. We consider these values to be the most accurate, although there are widely varying values for the capture cross sections in the literature, and further refinement may occur in the future. The values for FeGa and FeIn are less certain than those for Fe_i and FeB. Note that under illumination, Fe-acceptor pairs are dissociated, and so only interstitial Fe occurs in a working solar cell. However, the Fe-acceptor pairs lead to useful meta-stable properties that can be exploited for characterization purposes, as described below.

An important feature of isolated (i.e. un-paired) interstitial Fe in silicon is that it only presents a single donor level in the band-gap of silicon. This means that it may only have either a positive or neutral charge state, leading in turn to a relatively large capture cross section for electrons, and a relatively small capture cross section for holes (see Table1). Since electrons are minority carriers in p-type silicon, and since the capture of minority carriers controls the recombination lifetime in low or mid injection (which are generally the operating conditions for silicon solar cells), the presence of interstitial Fe in p-type silicon causes a lower lifetime than in n-type silicon [10]. This is illustrated in Figure 1, which shows the calculated effective lifetime for n- and p-type silicon as a function of the interstitial Fe concentration [Fe_i] based on the values in Table 1. Here a doping concentration of 10^{16} cm^{-3} is assumed, and a generation rate of 0.1 suns is used, which approximates the injection level at maximum power point. The QSS-Model software was used for these simulations [11], assuming a thermal velocity of 1.1×10^7 cm/s [12]. Auger recombination [13] is also included in the calculation, which causes the saturation at lower Fe concentrations. Clearly there is a large difference in the recombination activity of Fe_i in n- and p-type silicon, courtesy of the capture cross section asymmetry. This provides an incentive to consider the use of n-type silicon for solar cells in which dissolved iron impurities may be dominant. However, the presence of other recombination active defects, and the effective external gettering of dissolved iron during cell processing, mean that this condition may not often be satisfied in practice.

Detecting interstitial iron by lifetime measurements

Courtesy of the linear nature of Shockley-Read-Hall statistics, measurement of the carrier diffusion length or lifetime both before and after FeB pair dissociation allows the total dissolved Fe concentration to be determined [14]. The original method developed by Zoth and Bergholz [14] was based on surface photovoltage (SPV) measurements of the minority carrier diffusion length. The

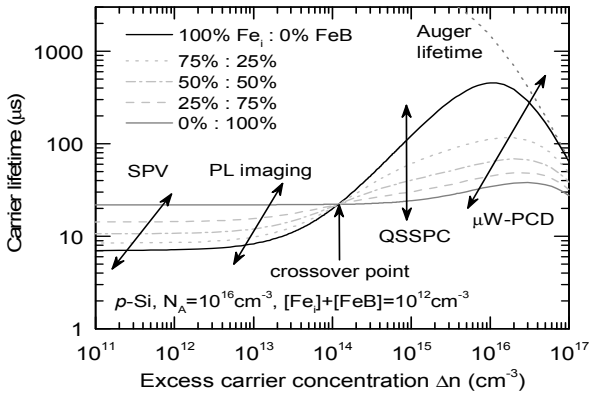

Fig 2. *Modelled effective lifetimes for Fe_i and FeB pairs, and combinations of the two, as a function of excess carrier density.*

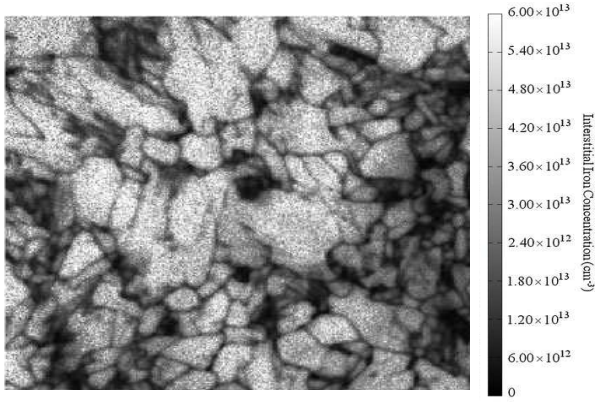

Fig 3. *Interstitial Fe concentrations in an as-cut multicrystalline silicon wafer based on PL images. Sample width is 7cm.*

approach was later extended to microwave photoconductance decay (μW-PCD) lifetime measurements, and then to quasi-steady-state photoconductance (QSSPC) data [15]. These methods are based on the same principle, but operate at different injection levels [9], and are extremely sensitive, in many cases capable of detecting dissolved Fe concentrations below 10^{10} cm^{-3}.

Figure 2 shows modelled injection dependent lifetimes for Fe_i and FeB in boron-doped p-type silicon with a dopant concentration of N_A=10^{16} cm^{-3}, using the recombination parameters of Table 1. The total Fe concentration, [Fe_i] + [FeB] is set to a value of 10^{12} cm^{-3}. Lifetimes for complete pair formation (100% FeB pairs) and complete pair dissociation (100% Fe_i) are shown, as are three intermediate cases having various combinations of Fe_i and FeB. The figure shows the excess carrier density ranges over which the various methods for measuring the change in carrier lifetime or diffusion length operate (SPV, μW-PCD, QSSPC and Photoluminescence (PL) imaging). Note that pair dissociation results in an increase in lifetime in high injection, and a decrease in low injection, with the curves exhibiting a crossover point near 10^{14} cm^{-3}. The position of this crossover point is weakly dependent on the base doping [8], and can be used as an unambiguous fingerprint for Fe contamination in device fabrication.

The FeB pairs may be dissociated thermally or by illumination. The pairs then re-form in the dark at room temperature as the interstitial Fe atoms diffuse and bond with the fixed B atoms, resulting in a time-sequence of lifetime curves such as those shown in Figure 2, until complete pair formation is achieved. The time constant of this pairing reaction is inversely proportional to the boron concentration [16], and for a doping concentration of 10^{16} cm^{-3} is approximately 35 minutes at 300 K [17]. Measuring this decay constant therefore provides another convenient fingerprint for Fe contamination. Interestingly, since the decay constant is determined by the concentration of ionized acceptor atoms, this method can be used to measure the acceptor concentration in compensated wafers [18], which is otherwise not easily obtained by conventional resistivity measurements.

Recently, high resolution PL imaging of carrier lifetimes in silicon wafers has been developed [19]. Such lifetime images taken before and after FeB pair dissociation can be used to generate a high resolution interstitial Fe image, taking care of the impact of variations in injection level [9]. An example of such an Fe image is shown in Figure 3. This as-cut wafer exhibits lower dissolved Fe concentrations near the grain boundaries and dislocation clusters, revealing internal gettering of Fe to those defects during ingot cooling [20]. This is a powerful method for studying precipitation and dissolution of Fe at extrinsic defects, both during ingot cooling and during cell processing [21,22], although care needs to be taken to minimize PL measurement artefacts near high recombination sites [22]. The following section examines such internal gettering in more detail.

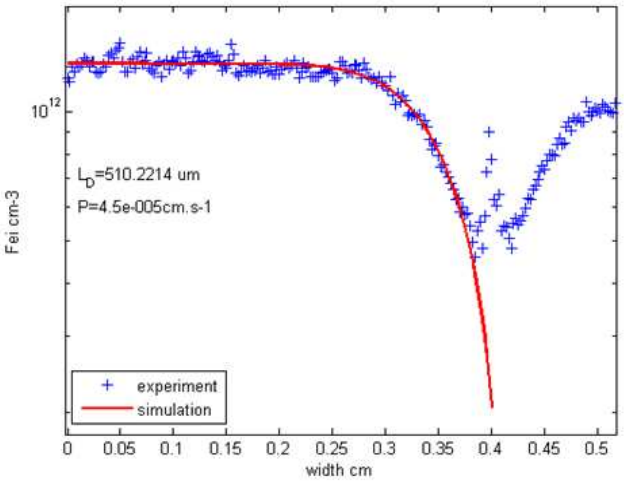

Fig 4. *Linescan of the interstitial Fe concentration near a grain boundary in a multicrystalline silicon wafer which was annealed at low temperature. The red line shows a simple diffusion model fitted to the data, yielding a diffusion length of Fe during the precipitation process of 510 microns, and a precipitation velocity of* 4.5×10^{-5} *cm/s.*

Internal gettering of iron

The dissolved Fe image in Figure 3 shows reduced interstitial iron concentrations at grain boundaries, appearing as lines, and also at dislocation clusters, appearing as dark regions extending in two dimensions. The extent of this internal gettering during ingot cooling depends on the dissolved Fe concentration, and also on the density of precipitation sites, both of which are strongly affected by the position of the wafer in the ingot [20,22].

We have developed a simple model for the precipitation of Fe at grain boundaries [22], in which there are three independent fit parameters: the dissolved Fe concentration far from the grain boundary, which is determined from the experimental data; the diffusion length of dissolved Fe in silicon during the precipitation process (either during ingot cooling, or during a fixed temperature anneal), which should be determined by the known diffusivity of Fe in silicon; and the precipitation velocity, *P*, which determines the propensity of the particular grain boundary to precipitate Fe atoms that reach it. In general *P* is likely to be a function of temperature. This is directly analogous to the generation, diffusion and recombination of excess carriers at a surface in a silicon wafer, where the precipitation velocity is the equivalent of the surface recombination velocity.

Figure 4 shows a linescan of the measured dissolved Fe concentration near a grain boundary in a mc-Si wafer [23] after annealing at low temperature (530 °C for one and a half hours, and then 600 °C for two and a half hours), and the simple model fitted to the data. The narrow hump in the Fe concentration data very close to the grain boundary is evidently an experimental artefact caused by either diffusion of carriers or scattering of emitted photons in the sample close to the grain boundary, or a combination of both [22]. The impact of scattered photons in the sample can be reduced by using a short-pass filter to eliminate the most weakly absorbed photons, although at the cost of some signal strength. In any case, this 'hump' region is excluded from the fit procedure. The model describes the remainder of the data well, and in this case yields a diffusion length for Fe during the precipitation process of 510 μm, which is close to the expected value of 470 μm based on the diffusivity of Fe during the anneal step [23].

Figure 5 shows more linescans from another sample after different annealing steps. These and other similar results are described in more detail elsewhere [24,25]. The plot on the left gives an absolute scale for the Fe concentration, while on the right the Fe concentrations are normalised. Several interesting features can be seen in these plots. Firstly, for high temperature anneals above 900 °C, the solubility limit of Fe is higher (above 2×10^{13} cm^{-3}) than the dissolved Fe concentration in the wafer (around 1×10^{13} cm^{-3}). Therefore there is no driving force for precipitation at the grain boundaries, and the Fe concentration becomes homogenised due to the diffusion of the dissolved Fe within the grains. It is also possible that there is some dissolution of Fe from the grain boundaries themselves, although this does not lead to any significant increase in the average dissolved Fe concentration, and so does not have a large impact (this effect may be more important in wafers with lower initial dissolved Fe concentrations).

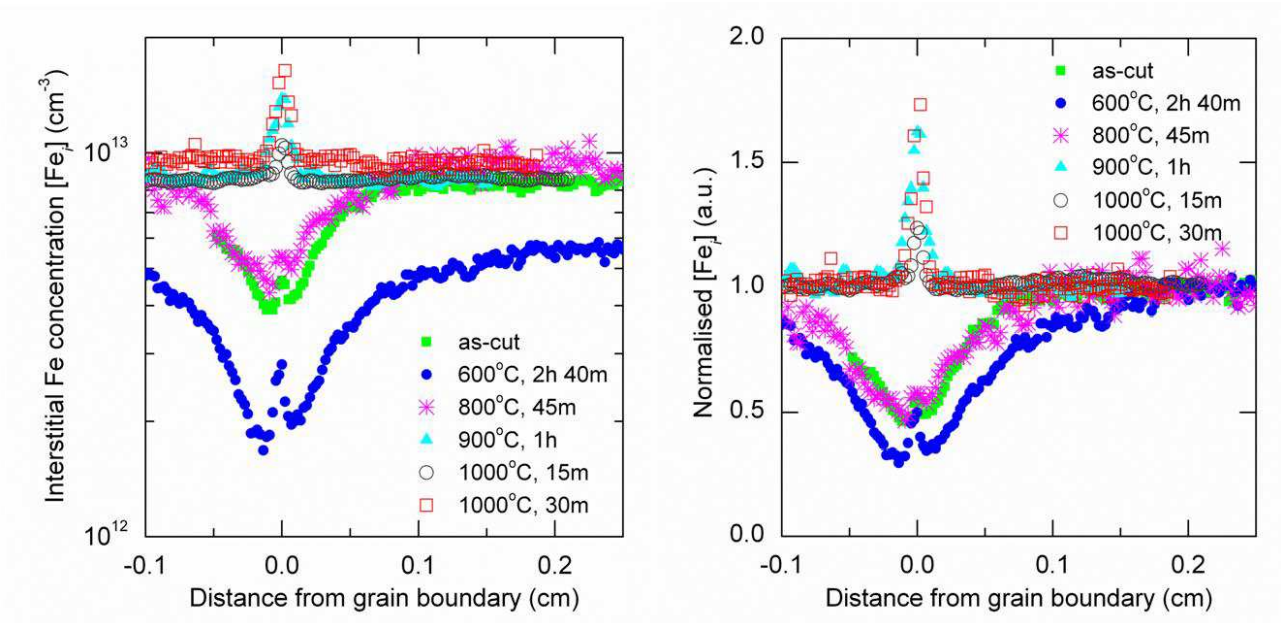

Fig 5. *Linescans of the interstitial Fe concentration near a grain boundary in a mc-Si wafer after various annealing steps. The left hand plot shows the absolute interstitial Fe concentration, while the right hand plot is normalised far from the grain boundary, in order to allow changes in the relative width and depth denuded zone near the grain boundary to be more easily seen.*

Secondly, during a low temperature anneal at 600 °C, there is a clear reduction in the dissolved Fe concentration across the wafer. The plot on the left shows that this occurs even far away from the grain boundaries, indicating precipitation at defects within the grains, as detailed elsewhere [24,25]. This precipitation at intra-grain defects is the most important in reducing the global dissolved Fe concentration during low temperature annealing, since the intra-grain regions account for a large majority of the wafer surface. The plot on the right shows that the width and relative depth of the denuded zone around the grain boundary is also increased, revealing precipitation of Fe at the grain boundary too. This is not surprising, since the solubility limit at this anneal temperature (around 5×10^{10} cm^{-3}) is far below the dissolved iron concentration, leading to supersaturated conditions, and providing a strong impetus for precipitation. At the intermediate anneal temperature of 800 °C, the solubility limit (around 5×10^{12} cm^{-3}) is only slightly below the dissolved iron concentration, resulting in no detectible precipitation.

External gettering of iron

Most p-type cells have a phosphorus diffusion to form the *p-n* junction on the front side. This heavily doped region is effective at gettering dissolved Fe from the silicon bulk, courtesy of the greater solubility of Fe in the highly doped region. However, the gettering effectiveness depends strongly on the gettering temperature, primarily because of the rapid divergence of the solubility limits of Fe in the diffused regions compared to the bulk region as the temperature is reduced. Figure 6 summarizes some of our recent results on gettering of Fe in deliberately contaminated monocrystalline silicon wafers [26,27]. After phosphorus diffusions performed between 780 – 850 °C, only 3-9% of the initial dissolved Fe concentration remains (details are in Ref [27]). Adding a low temperature anneal at 650 °C reduces the initial Fe concentration further to around 0.1% of the initial value, precisely due to the greater ratio of solubility limits between the gettering layer and the bulk at lower temperatures. Phosphorus gettering is also strongly affected by the phosphorus concentration in the diffused region. Reducing the peak phosphorus concentration from 2×10^{20} cm^{-3} to 3×10^{19} cm^{-3} leads to a reduction in gettering efficiency of around an order of magnitude, despite the total phosphorus concentration remaining largely unchanged [28].

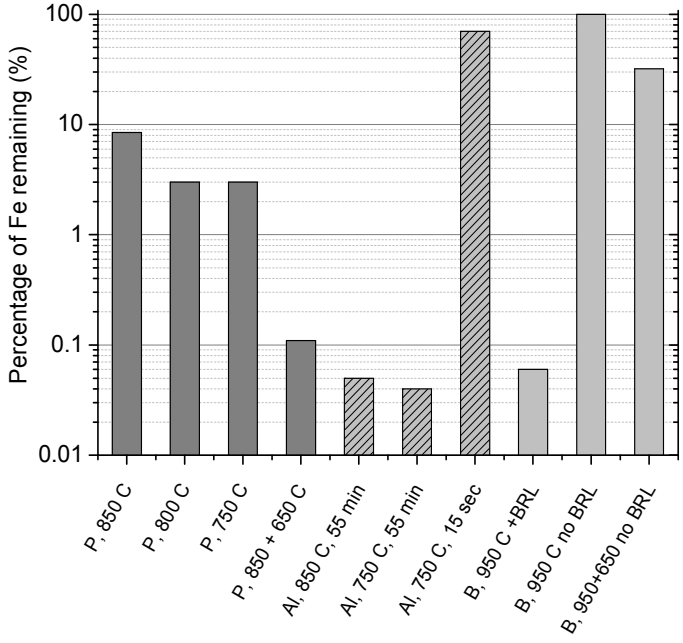

Fig 6. *Fe gettering effectiveness for phosphorus (P), aluminium (Al) and boron (B) diffused regions for different diffusion conditions as explained in the text.*

Aluminium gettering is even more effective at removing Fe, as seen in Figure 6, leaving around 0.05% of the Fe after annealing at 750-850 °C for 55 minutes, without the need for a subsequent low temperature anneal. However, Al diffusions on the rear side of solar cells, which are used to form the so-called Back Surface Field (BSF), are usually very rapid, typically remaining at the peak temperature for only a few seconds. As shown in Fig 6, 15 seconds of annealing at 750 °C still leaves 70% of the dissolved Fe in the base, revealing that the time is not long enough for the Fe to reach the gettering site, as confirmed by modelling [27]. Such alloyed aluminium regions may be effective at removing impurities from close to the rear surface, but this is unlikely to have much impact on the performance of a front junction solar cell.

Gettering by boron diffusions is more complex than phosphorus or aluminium gettering. During boron diffusion, a so-called boron-rich layer (BRL) usually forms at the interface between the boron-doped silicon and the boro-silicate glass. This BRL layer is a very effective gettering site. If the BRL is left intact during cooling of the sample, the gettering is excellent, leaving less than 0.1% of the Fe, similar to Al, as shown in Figure 6. However, if the BRL is oxidized out at high temperature, as is normally the case in order to allow high quality surface passivation, the Fe is almost completely re-injected from the BRL into the wafer bulk, resulting in no detectible reduction in the bulk Fe concentration (as shown in the second-last column of Figure 6). In this case, even a subsequent low temperature anneal at 650 °C still leaves about 30% of the initial Fe. Two approaches to avoid this problem have been demonstrated recently – the first is to remove the BRL chemically at low temperature after the wafer is extracted from the diffusion furnace [26,29], or to subsequently apply a light phosphorus diffusion on top of the underlying boron diffusion [28].

Acknowledgements

This research has been supported by the Australian Research Council through the Future Fellowships program.

References

[1] T. Buonassisi*, et al.*, Chemical natures and distributions of metal impurities in multicrystalline silicon materials, Progress in Photovoltaics: Research and Applications, 14, (2006) 513.

[2] E. Olsen and E. J. Øvrelid, Silicon nitride coating and crucible - effects of using upgraded materials in the casting of multicrystalline silicon ingots, Progress in Photovoltaics: Research and Applications, 16, (2007) 93.

[3] A. A. Istratov, T. Buonassisi, R. J. McDonald, A. R. Smith, R. Schindler, J. A. Rand, J. P. Kalejs and E. R. Weber, Metal content of multicrystalline silicon for solar cells and its impact on minority carrier diffusion length, Journal of Applied Physics, 94, (2003) 6552.

[4] D. Macdonald, A. Cuevas, A. Kinomura, Y. Nakano and L. J. Geerligs, Transition metal profiles in a multicrystalline silicon ingot, Journal of Applied Physics, 97, (2005) 033523.

[5] T. Buonassisi, *et al.*, Synchrotron-based investigations of the nature and impact of iron contamination in multicrystalline silicon solar cells, Journal of Applied Physics, 97, (2005) 074901.

[6] J. Schmidt and D. Macdonald, Recombination activity of iron-gallium and iron-indium pairs in silicon, Journal of Applied Physics, 97, (2005) 113712.

[7] A. A. Istratov, H. Hieslmair and E. R. Weber, Iron and its complexes in silicon, Applied Physics A, 69, (1999) 13.

[8] D. Macdonald, T. Roth, P. N. K. Deenapanray, T. Trupke and R. A. Bardos, Doping dependence of the carrier lifetime crossover point upon dissociation of iron-boron pairs in crystalline silicon, Applied Physics Letters, 89, (2006) 142107.

[9] D. Macdonald, J. Tan and T. Trupke, Imaging interstitial iron concentrations in boron-doped crystalline silicon using photoluminescence, Journal of Applied Physics, 103, (2008) 073710.

[10] D. Macdonald and L. J. Geerligs, Recombination activity of iron and other transition metal point defects in n- and p-type crystalline silicon, Applied Physics Letters, 85, (2004) 4061.

[11] A. Cuevas, Modelling silicon characterisation, Energy Procedia, 8, (2011) 94.

[12] W. M. Bullis and H. R. Huff, Interpretation of carrier recombination lifetime and diffusion length measurements in silicon, J. Electrochem. Soc., 143, (1996) 1399.

[13] M. J. Kerr and A. Cuevas, General parameterization of Auger recombination in crystalline silicon, Journal of Applied Physics, 91, (2002) 2473.

[14] G. Zoth and W. Bergholz, A fast, preparation-free method to detect iron in silicon, Journal of Applied Physics, 67, (1990) 6764.

[15] D. Macdonald, L. J. Geerligs and A. Azzizi, Iron detection in crystalline silicon by carrier lifetime measurements for arbitrary injection and doping, Journal of Applied Physics, 95, (2004) 1021.

[16] H. Reiss, C. S. Fuller and F. J. Morin, Chemical interactions among defects in germanium and silicon, Bell System Technical Journal, 35, (1956) 535.

[17] J. Tan, D. Macdonald, F. Rougieux and A. Cuevas, Accurate measurement of the formation rate of iron–boron pairs in silicon, Semiconductor Science and Technology, 26, (2011) 055019.

[18] D. Macdonald, A. Cuevas and L. J. Geerligs, Measuring dopant concentrations in compensated p-type crystalline silicon via iron-acceptor pairing, Applied Physics Letters, 92, (2008) 202119.

[19] T. Trupke, R. A. Bardos, M. C. Schubert and W. Warta, Photoluminescence imaging of silicon wafers, Applied Physics Letters, 89, (2006) 044107.

[20] A. Liu, Y.-C. Fan and D. Macdonald, Interstitial iron concentrations across multicrystalline silicon wafers via photoluminescence imaging, Progress in Photovoltaics: Research and Applications, 19, (2011) 649.

[21] T. Buonassisi, *et al.*, Impact of metal silicide precipitate dissolution during rapid thermal processing of multicrystalline silicon solar cells, Applied Physics Letters, 87, (2005) 121918.

[22] A. Y. Liu, D. Walter, S. P. Phang and D. Macdonald, Investigating internal gettering of iron at grain boundaries in multicrystalline silicon via photoluminescence imaging, IEEE Journal of Photovoltaics, 2, (2012) 479.

[23] A. Liu, D. Walter, S. P. Phang and D. Macdonald, Imaging and modelling the internal gettering of interstitial iron by grain boundaries in multicrystalline silicon, 38th IEEE Photovoltaic Specialists Conference (2012) 248.

[24] A. Y. Liu, D. Walter and D. Macdonald, Investigating precipitation and dissolution of iron in multicrystalline silicon wafers during annealing, 22nd International Photovoltaic Science and Engineering Conference (2012)

[25] A. Liu and D. Macdonald, Precipitation of interstitial iron in multicrystalline silicon, this publication, (2013).

[26] S. P. Phang, W. Liang, B. Wolpensinger, M. A. Kessler and D. Macdonald, Trade-offs between impurity gettering, bulk degradation, and surface passivation of boron rich layers on silicon solar cells, IEEE Journal of Photovoltaics, 3, (2013) 261.

[27] S. P. Phang and D. Macdonald, Direct comparison of boron, phosphorus and aluminum gettering of iron in crystalline silicon, Journal of Applied Physics, 109, (2011) 073521.

[28] S. P. Phang and D. Macdonald, Effect of boron co-doping and phosphorus concentration on phosphorus diffusion gettering, IEEE Journal of Photovoltaics, (2013) submitted.

[29] K. Ryu, A. Upadhyaya, H. J. Song, C. J. Choi, A. Rohatgi and Y. W. Ok, Chemical etching of boron-rich layer and its impact on high efficiency n-type silicon solar cells, Applied Physics Letters, 101, (2012) 073902.